On the Accuracy of Surface Scattering Theories – Supplemental

Matthew Avolio[1], Eugene D'Eon[2], Shlomi Steinberg[1]

[1]University of Waterloo [2]Nvidia

1 Reference Photo Setup

Lacking a gonioreflectometer, we created a photo acquisition setup (Fig. 1) to directly compare real surface reflections to renderings. The surface is illuminated from a checker board textured plane that projects diffuse and incoherent light from a tungsten lamp onto the surface. This minimizes the appearance of glints from scratches while also spreading it over a large surface area reducing the distraction of the spatially varying roughness. A 2700 K tungsten lamp was used as its colour spectrum is well approximated by a blackbody emitter. The spectrum is important as optical roughness in diffractive scattering models is dependent on the wavelength of incident light. An ArUco marker [GJMSMCMJ14] is placed in the center of the cutting mat and is used to estimate the camera extrinsic parameters for the renderings. Photos from the camera are edited to remove barrel distortion and colour corrected with a colour checker. We render a scene with the same colour squares and edit to match with some liberties taken to compensate for a mismatch in the response of the virtual and real sensor.

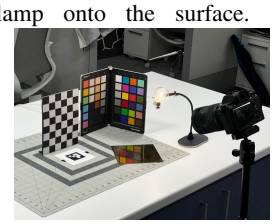

Figure 1: Photo setup.

2 Rendering

We measure the scene geometry directly from the acquisition setup and use the camera pose estimated from the ArUco marker. Metals are described using wavelength-dependent refractive indices [Pol24], and illumination is a 2700 K blackbody point light in Mitsuba [JSR*22].

2.1 Rendering the GHS BRDF

The full GHS BRDF is as follows:

$$\mathrm{BRDF}_{\mathrm{GHS}}\left(\hat{\mathbf{i}},\hat{\mathbf{o}}\right) = R\sum_{m=0}^{\infty}\frac{e^{-g}g^m}{\sigma_h^2 m!}P_{\mathrm{KC}}\left(\vec{\zeta}^{\perp}\right)^{\star m}, \tag{1}$$

which is an infinite Poisson-weighted sum of self-convolutions of the normalized PSD. In practice, the series is truncated to diffraction orders m within three standard deviations of the mean g.

The higher-order self-convolution terms $P_{\mathrm{KC}}^{\star m}$, for $m \geq 1$, do not admit closed form expressions for arbitrary γ. Instead, since P_{KC} is nearly stable under convolution, they are approximated by precomputing the convolutions using:

$$P_{KC}^{\star m} = \frac{1}{2\pi}\mathcal{H}_0\{C_{KC}^m\}\,, \tag{2}$$

where $\mathcal{H}_0$ denotes the zeroth-order Hankel transform and C_{KC} is the KC ACV. The resulting KC PSD is then refit with a free correlation length L_c. For a specific PSD, the refit correlation length scales as a power law $L_c\, m^{-x}$ where x is a fitted parameter (Fig. 2). While imperfect, this allows for evaluating and sampling the higher-order terms in the same way as the first.

To sample Eq. 1, an order m is sampled from the Poisson distribution using Knuth's algorithm [Knu97]. Then, the modified KC PSD is sampled using the same routine as described by Holzschuch and Pacanowski [HP17]. Given uniform variates $u_1, u_2 \in [0,1)$, let:

$$f = \frac{1}{L_c}\sqrt{(1-Mu_1)^{-\frac{2}{\gamma-1}}-1} \tag{3}$$

$$M = 1-\left[1+k^2L_c^2(1+\sin\theta_i)^2\right]^{-\frac{\gamma-1}{2}}. \tag{4}$$

Then,

$$\phi_{\max} = \arccos\max\left\{-1,\ \frac{(f/k)^2+\sin^2\theta_i-1}{2(f/k)\sin\theta_i}\right\} \tag{5}$$

$$\phi_f = \phi_i + (2u_2-1)\,\phi_{\max}\,, \tag{6}$$

where ϕ_i is the azimuth of the incident direction $\hat{\mathbf{i}}$. Now, given $\hat{\mathbf{i}}$ and wavenumber k, an importance-sampled direction is:

$$\hat{\mathbf{o}} = \frac{1}{k}\vec{\zeta}-\hat{\mathbf{i}}\,, \tag{7}$$

$$\text{where}\qquad \vec{\zeta} = f(\cos\phi_f,\ \sin\phi_f)^{\top}\,. \tag{8}$$

The computed $\vec{\zeta}$ is the wave-optical equivalent of the "half vector".

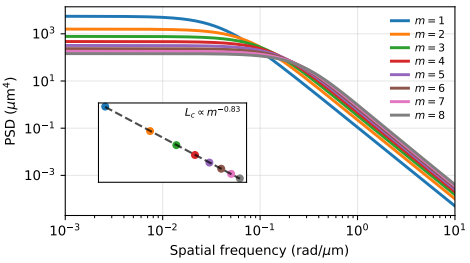

Figure 2: Self convolutions of P_{KC} with m denoting convolution order. Inset: log-log plot of refitted correlation lengths L_c.

Full Comparison: View 1

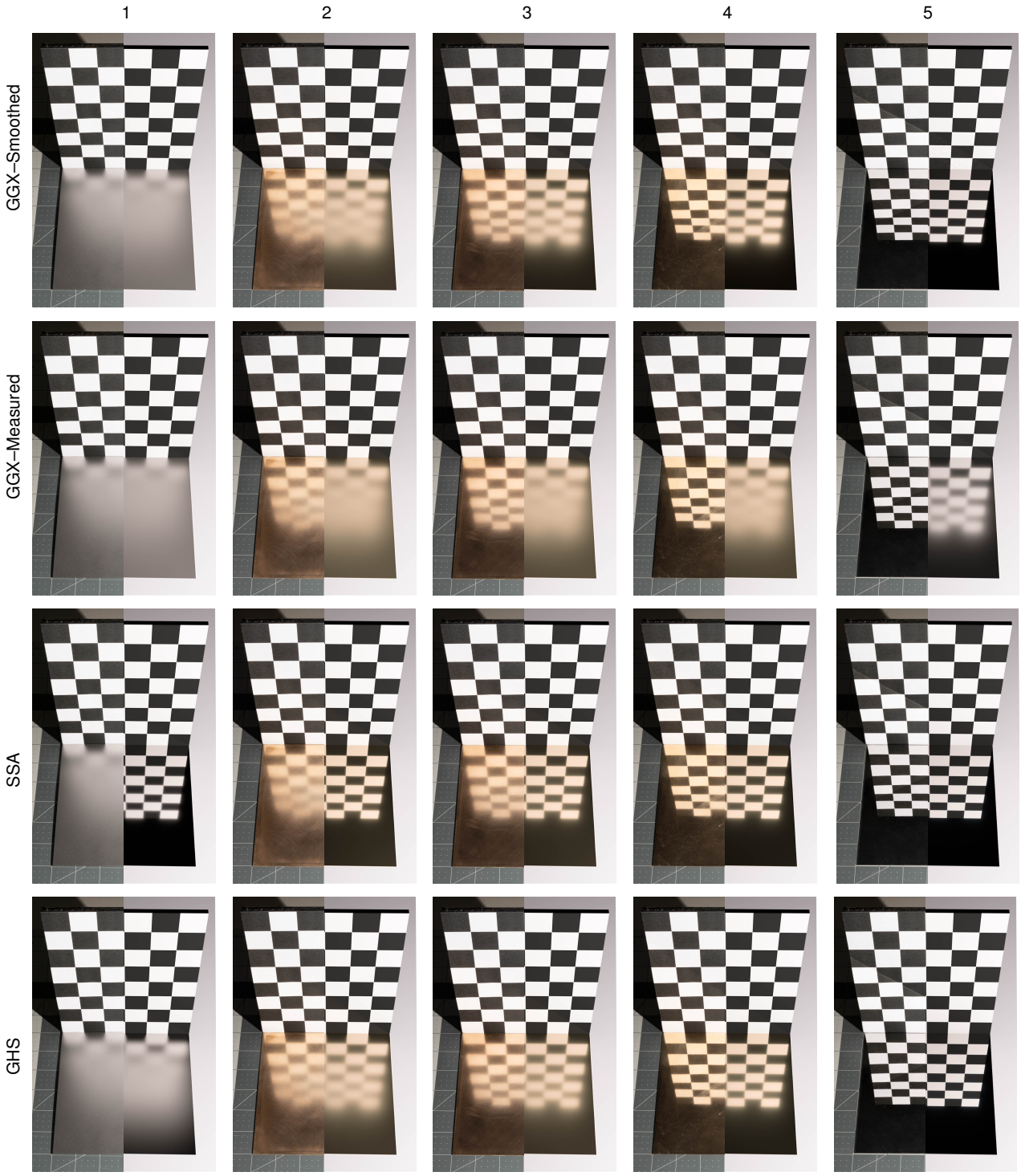

Figure 3: Reference photos compared to GGX (Gaussian smoothed and measured), SSA GHS (SSA), and full GHS predictions.

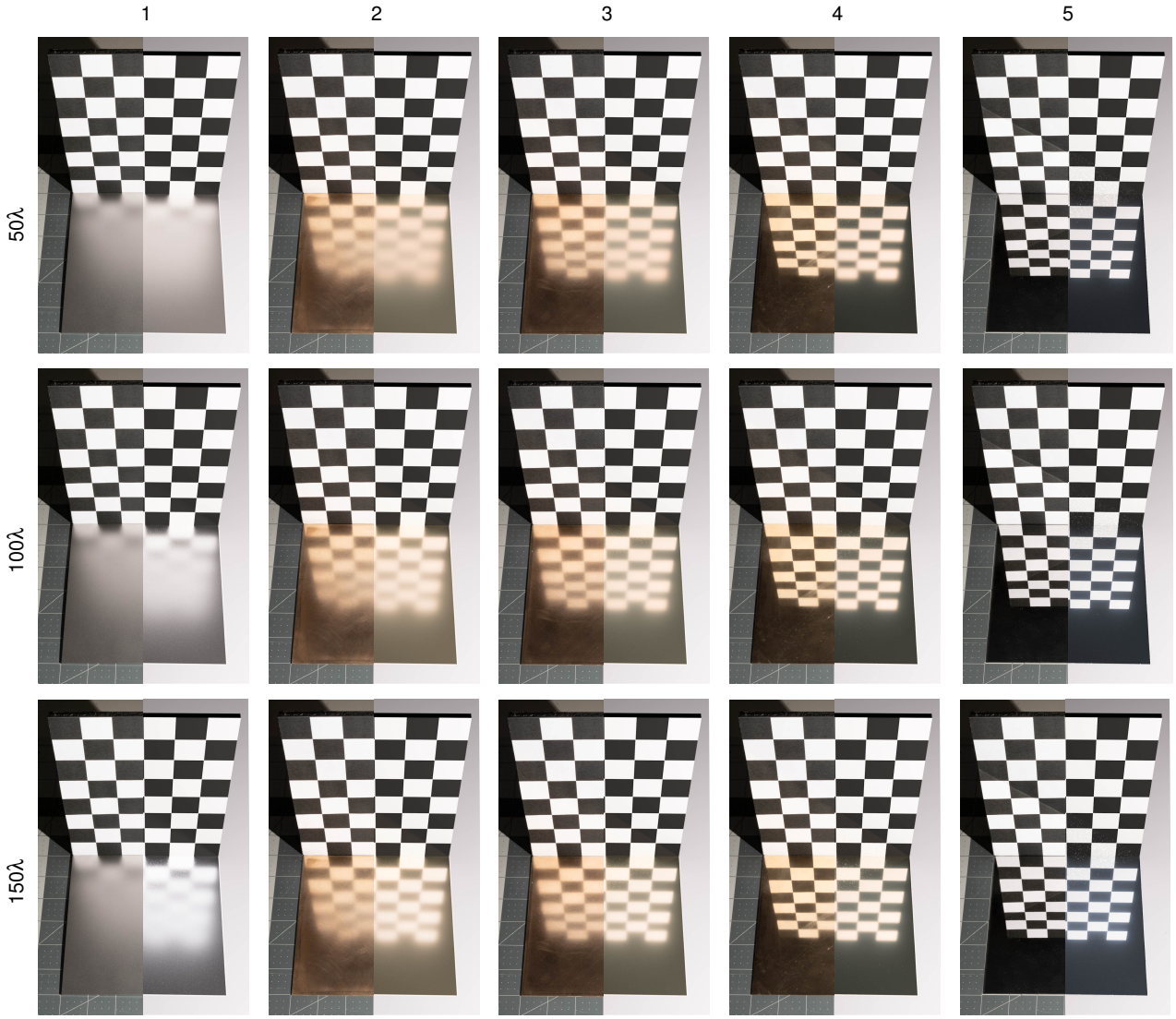

Figure 4: Two-scale model with low-pass filter macro-roughness cutoffs of at 50λ, 100λ, and 150λ

Full Comparison: View 2

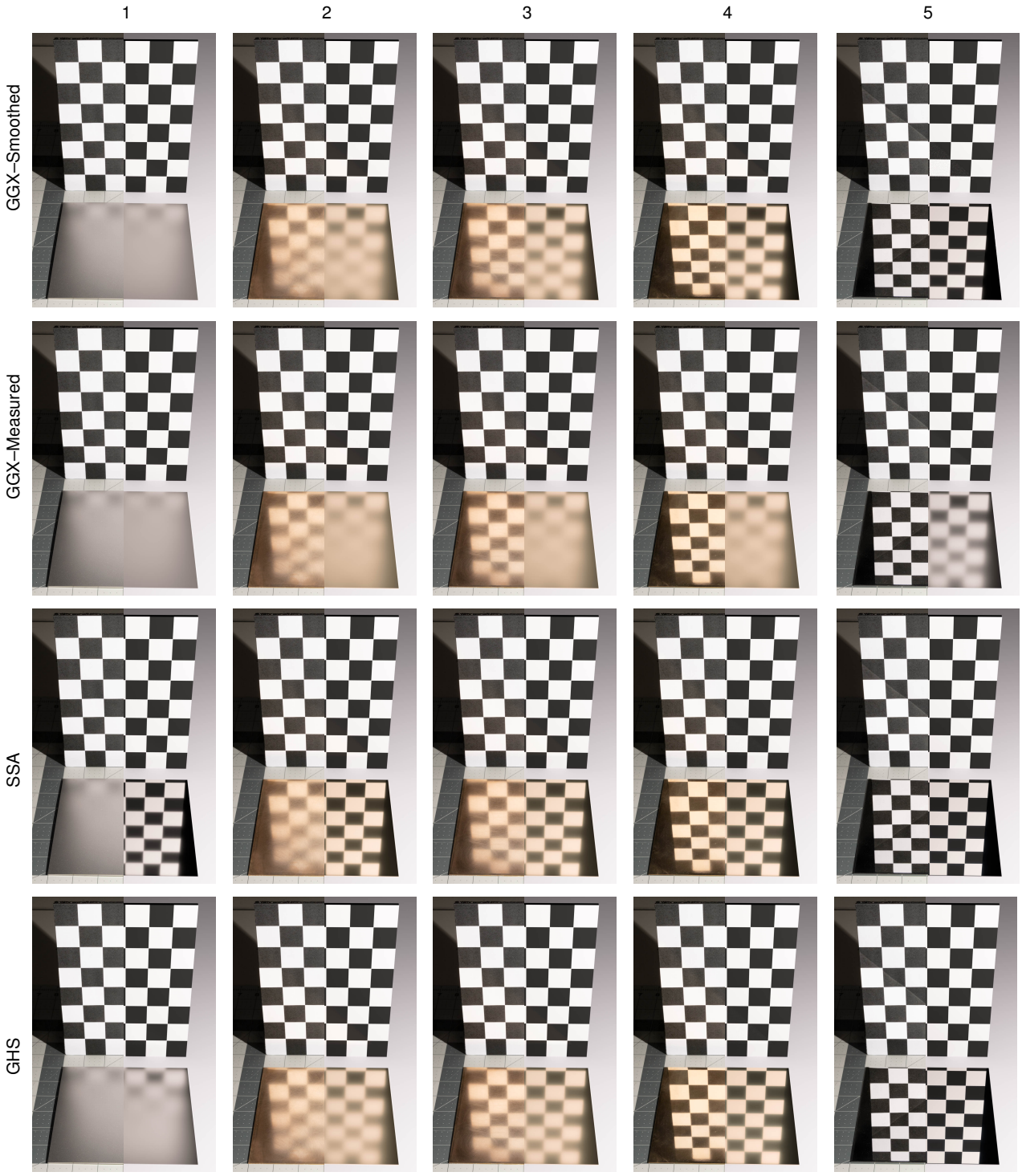

Figure 5: Reference photos compared to GGX (Gaussian smoothed and measured), SSA GHS (SSA), and full GHS predictions.

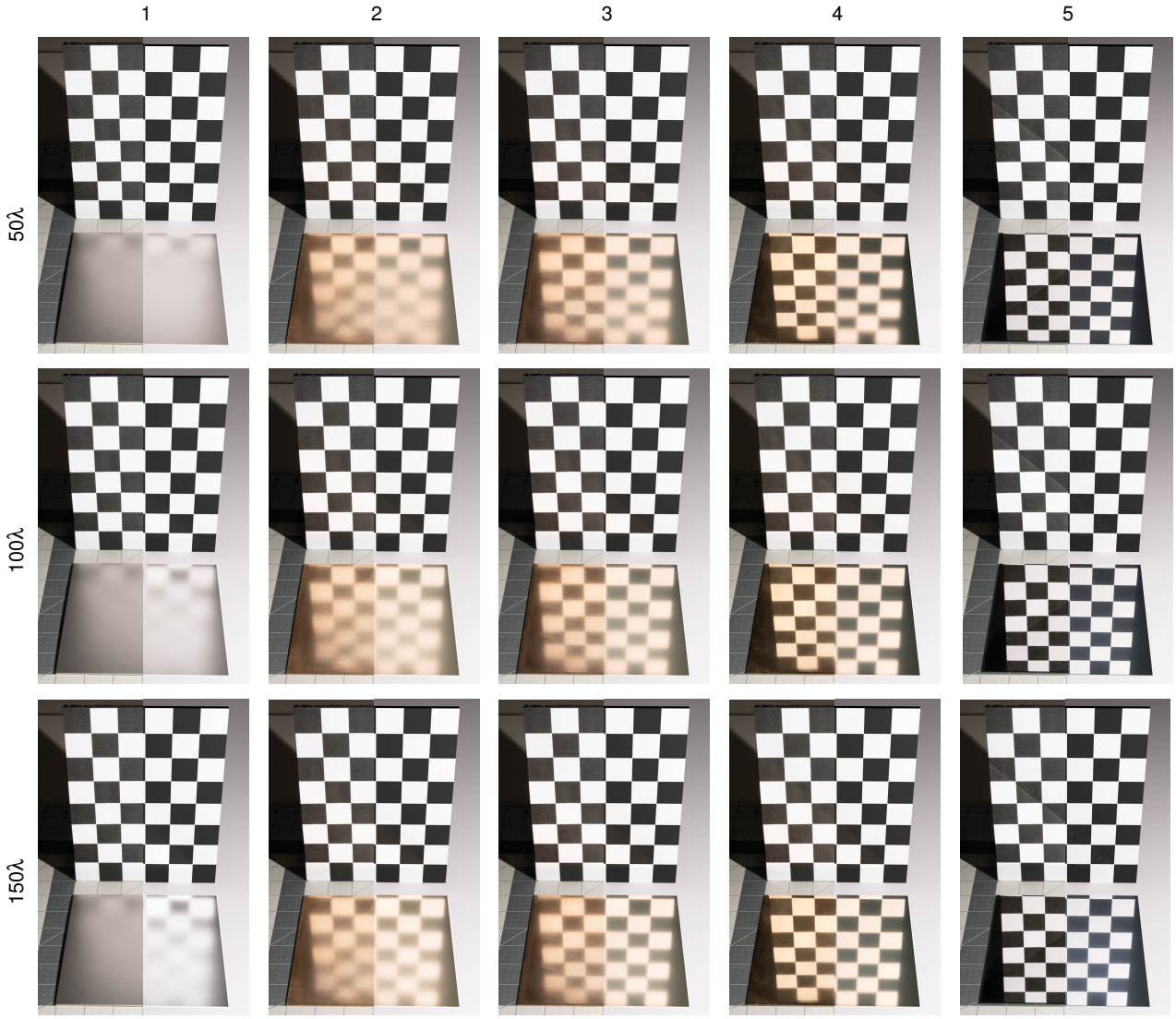

Figure 6: Two-scale model with low-pass filter macro-roughness cutoffs of at 50λ, 100λ, and 150λ

Full Comparison: View 3

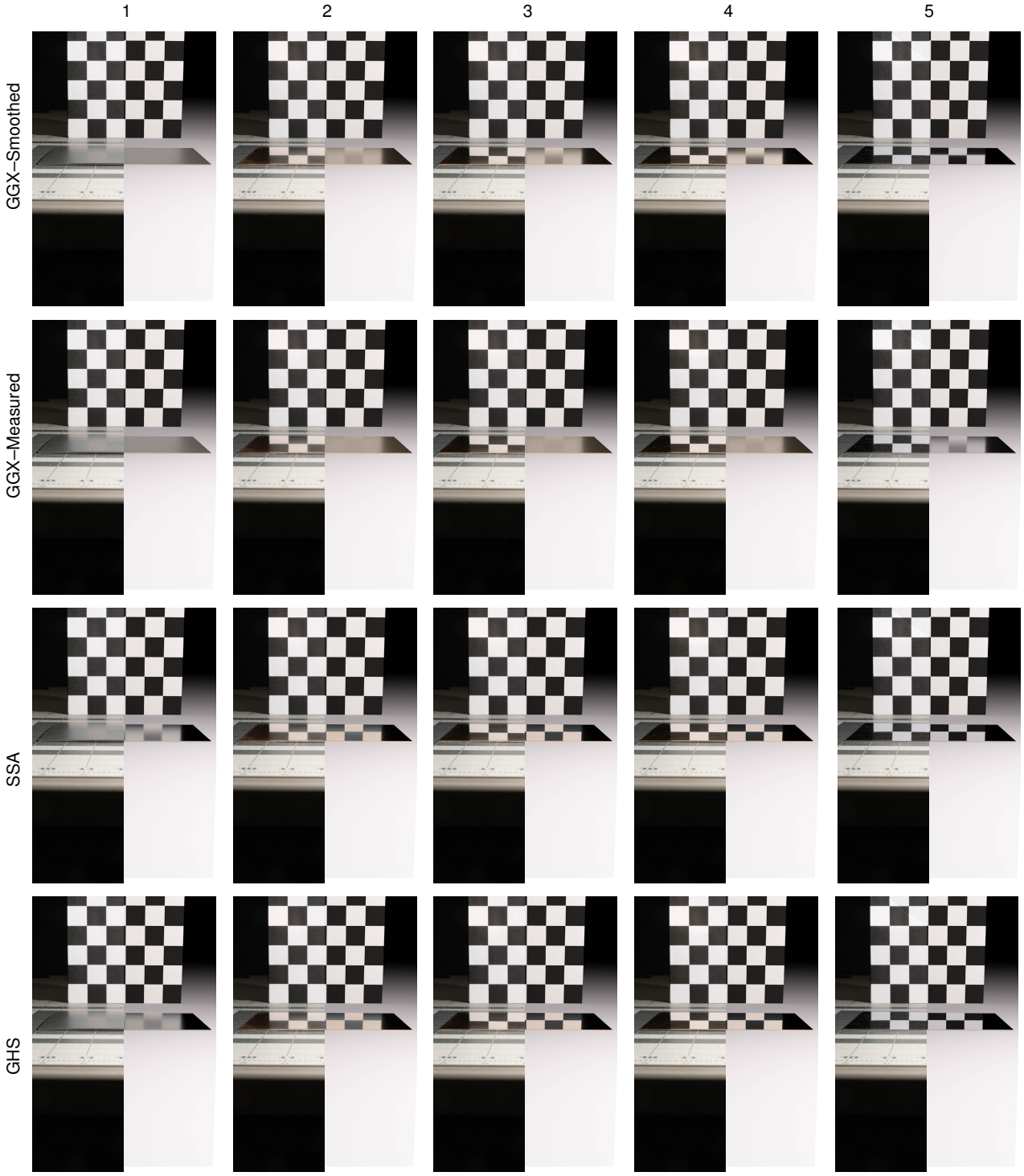

Figure 7: Reference photos compared to GGX (Gaussian smoothed and measured), SSA GHS (SSA), and full GHS predictions.

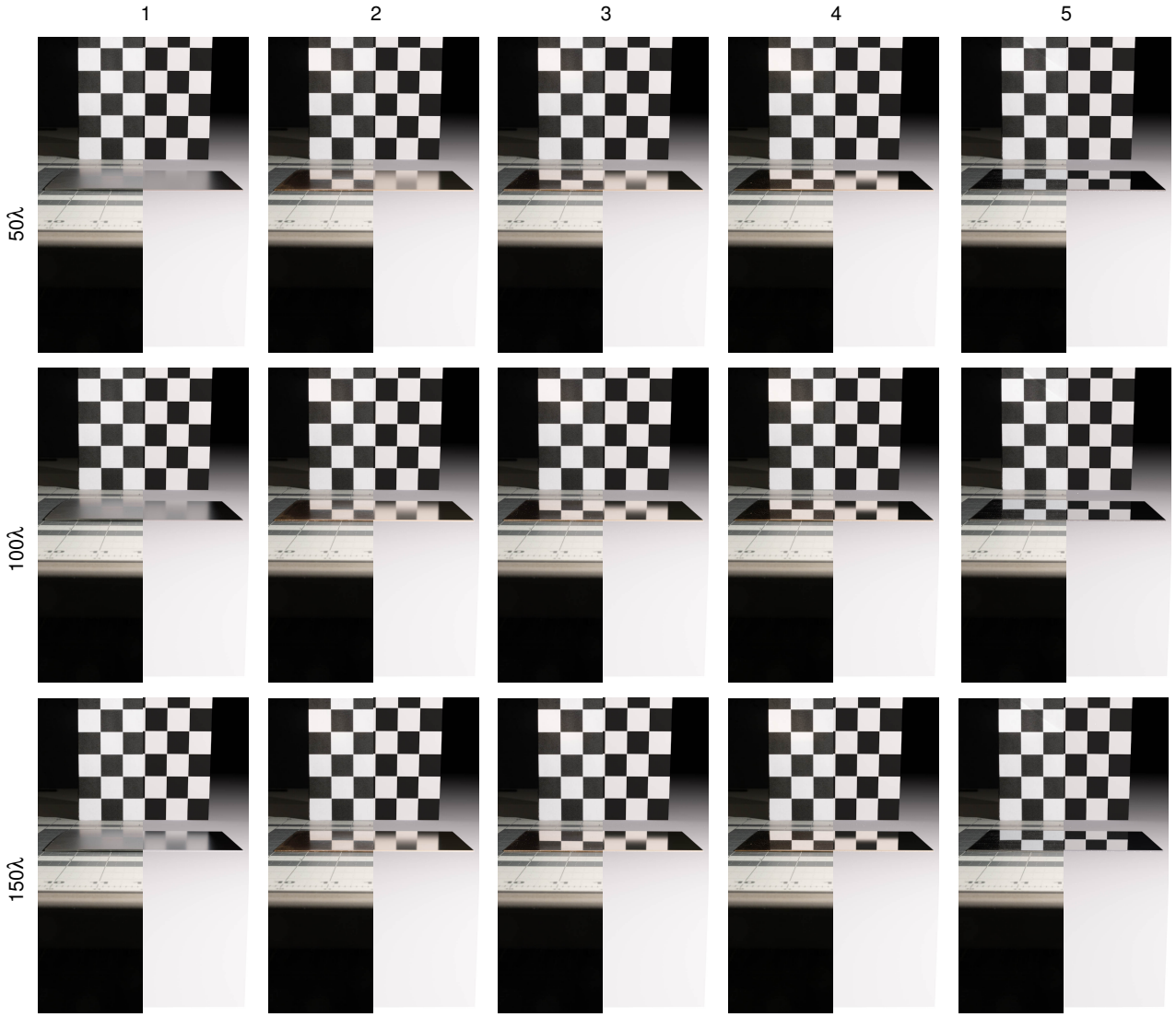

Figure 8: Two-scale model with low-pass filter macro-roughness cutoffs of at 50λ, 100λ, and 150λ

References

[GJMSMCMJ14] GARRIDO-JURADO S., MUÑOZ-SALINAS R., MADRID-CUEVAS F., MARÍN-JIMÉNEZ M.: Automatic generation and detection of highly reliable fiducial markers under occlusion. *Pattern recognition 47*, 6 (2014), 2280–2292. 1

[HP17] HOLZSCHUCH N., PACANOWSKI R.: A two-scale microfacet reflectance model combining reflection and diffraction. *ACM Trans. Graph. 36*, 4 (July 2017). URL: https://doi.org/10.1145/3072959.3073621, doi:10.1145/3072959.3073621. 1

[JSR*22] JAKOB W., SPEIERER S., ROUSSEL N., NIMIER-DAVID M., VICINI D., ZELTNER T., NICOLET B., CRESPO M., LEROY V., ZHANG Z.: Mitsuba 3 renderer, 2022. https://mitsuba-renderer.org. 1

[Knu97] KNUTH D. E.: *The art of computer programming. Volume 2, Seminumerical algorithms*, 3rd ed. ed. Addison Wesley, Place of publication not identified, 1997. 1

[Pol24] POLYANSKIY M. N.: Refractiveindex.info database of optical constants. *Scientific Data 11*, 1 (Jan 2024), 94. URL: https://doi.org/10.1038/s41597-023-02898-2, doi:10.1038/s41597-023-02898-2. 1